Synthesis of a Cauer Equivalent Circuit for Electric Devices From Computed and Measured Data

Yoshitsugu Otomo and Hajime Igarashi, *Member, IEEE*

***Abstract*—This article proposes a method for modeling electric devices based on a Cauer circuit whose circuit parameters are directly determined from measured or computed data using the adjoint variable method. It has been shown that electric devices that are governed by the quasi-static Maxwell's equation can be modeled by the Cauer circuit. From the synthesized Cauer circuit, eddy current losses can be evaluated for a wide frequency range. Moreover, it can be embedded into a circuit simulator to perform the time-domain analysis. It is shown that the Cauer circuit whose parameters are identified using the proposed method works better for a simple numerical model than that whose parameters are identified using a genetic algorithm. Moreover, the Cauer equivalent circuit of a reactor and a power inductor is synthesized from the measured data using the proposed method. It is shown that the input impedance of the reactor and power inductor is well approximated by the Cauer circuit over the frequency domain of interest.**

***Index Terms*—Adjoint variable method (AVM), Cauer equivalent circuit, curve fitting, litz wire, sensitivity analysis.**

I. Introduction

TO DOWNSIZE electric devices, such as transformers, electric motors, and inductors, the driving frequency has been increased, which has led to an increase in eddy current losses due to the skin and proximity effects. The finite element (FE) method can effectively compute the eddy currents, although its computational cost can be large because the device model has to be discretized into sufficiently fine elements that are smaller than the skin depth. In particular, repeated FE analysis in a design process can be unacceptably time consuming.

To accelerate computations, equivalent circuit models that consider the eddy current effects have been proposed. For example, the Cauer equivalent circuit of a steel sheet has been derived from the analytical solution to the quasi-static Maxwell's equations [1]–[3]. The Foster equivalent circuit of an inductor with arbitrary geometry has been synthesized using model order reduction [4], [5] applied to the FE equation of the quasi-static Maxwell's equation. It has been shown that the Cauer equivalent circuit can be derived from the Foster circuit via a rational polynomial representation [6]. Of note, the Cauer equivalent circuit has been directly derived from the FE equation of the 2-D and 3-D quasi-static Maxwell's equations [7], [8]. This means that a wide class of electric devices can be modeled using the Cauer circuit. In fact, it has been shown that permanent magnet synchronous motors and induction motors can be modeled by the Cauer circuit [9], [10]. Moreover, the electrochemical impedance of a diffusion and reaction process has been represented by the Cauer circuit [11]. With these approaches, the synthesized Cauer equivalent circuit can be embedded into circuit simulators and the time-domain analysis can be readily performed.

One can also determine the circuit parameters of the Cauer circuit by curve fitting. The parameters are determined so that the error between the input impedance of the equivalent circuit and that of the electric device of interest is minimized. The identification of equivalent circuit parameters using stochastic approaches, such as genetic algorithms (GAs), has been adopted because of their high search ability and versatility [12]–[16]. Moreover, the authors have successfully applied stochastic approach to the modeling of a wireless power transfer device [17], where the curve fitting was performed using a GA. One of the merits of the curve-fitting approach is that we only need the computed or measured input impedance of a device. This approach is especially effective when the FE analysis is ineffective but measurements are available, as in the case when there is uncertainty in the material properties or extremely fine structures, such as litz wire, are considered. A stochastic method would fail to uniquely determine the circuit parameters because of its stochastic nature unless a suitably weighted regularization term is introduced to the cost function [18]. Stochastic approaches also have a relatively high computational cost.

Sensitivity analysis based on the adjoint technique, which is a deterministic approach, has been used for circuit design and analysis [19]–[26]. Tellegen's approach, which uses an adjoint network, is widely used for circuit design [19]–[21]. It is also possible to directly compute the sensitivity of circuit equations based on the adjoint variable method (AVM) [22]–[26]. In particular, the complex AVM has been proposed for analyzing complex linear systems, such as *RL* circuits [25], [26]. Deterministic approaches are rather simple and have a smaller computational cost compared with that of stochastic approaches. As described above, there are many studies on the application of

Manuscript received March 20, 2020; revised June 30, 2020; accepted September 1, 2020. Date of publication September 7, 2020; date of current version November 20, 2020. This work was supported in part by the JSPS KAKENHI Grants JP19J20375 and JP18H01664 and in part by the MEXT Doctoral Program for the Data-Related InnoVation Expert Hokkaido University (D-DRIVE-HU) Program. Recommended for publication by Associate Editor K. Sheng. *(Corresponding author: Yoshitsugu Otomo.)*

The authors are with the Graduate School of Information Science and Technology, Hokkaido University, Sapporo 060-0814, Japan (e-mail: otomo@em.ist.hokudai.ac.jp; igarashi@ssi.ist.hokudai.ac.jp).

Color versions of one or more of the figures in this article are available online at https://ieeexplore.ieee.org.

Digital Object Identifier 10.1109/TPEL.2020.3022167

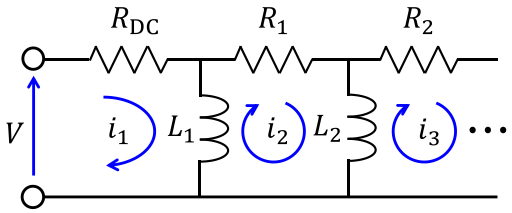

Fig. 1. Cauer equivalent circuit.

AVM to optimal design. However, there have been little studies to identify the circuit parameters using AVM. In particular, AVM has not been applied to identification of the Cauer circuit that has the above-mentioned engineering importance.

In this article, we propose a method for modeling electric devices based on a Cauer circuit whose circuit parameters are directly determined from either measured or computed data using AVM. To evaluate the effectiveness of the proposed method, we apply it to an FE model of a 20-turn inductor. Moreover, the proposed method is used to synthesize a Cauer circuit model from the measured data of a reactor and a power inductor.

II. Cauer Equivalent Circuit Representation

Let us consider the Cauer equivalent circuit shown in Fig. 1, which can be derived from the quasi-static Maxwell's equations to effectively evaluate the eddy current loss and perform dynamic simulation. The quasi-static Maxwell's equations in the Laplace domain can be written as

$$\mathrm{rot}\nu\ (\mathrm{rot}\boldsymbol{A}) + j\omega\sigma\,(\boldsymbol{A} + \mathrm{grad}\varphi) = \boldsymbol{J} \tag{1a}$$

$$\mathrm{div}\ \{j\omega\sigma\,(\boldsymbol{A} + \mathrm{grad}\varphi)\} = 0 \tag{1b}$$

where $\boldsymbol{A}$, φ, ν, j, ω, σ, and $\boldsymbol{J}$ denote the vector and scalar potentials, magnetic reluctivity, imaginary unit, angular frequency, electric conductivity, and current density, respectively. By applying the weighted residual method in conjunction with the Galerkin method to (1), we obtain

$$\sum_j A_j \left[\int_\Omega \mathrm{rot}\boldsymbol{N}_i \cdot \nu\mathrm{rot}\boldsymbol{N}_j d\Omega + j\omega\sigma \int_\Omega \boldsymbol{N}_i \cdot \boldsymbol{N}_j d\Omega\right] + j\omega\sigma \sum_k \varphi_k \int_\Omega \boldsymbol{N}_i \cdot \mathrm{grad}N_k d\Omega = I \int_\Omega \boldsymbol{N}_i \cdot \boldsymbol{j}_0 d\Omega \tag{2a}$$

$$j\omega\sigma \sum_j A_j \int_\Omega \boldsymbol{N}_j \cdot \mathrm{grad}N_u d\Omega + j\omega\sigma \sum_k \varphi_k \int_\Omega \mathrm{grad}N_k \cdot \mathrm{grad}N_u d\Omega = 0 \tag{2b}$$

where $\boldsymbol{N}_i$, N_i, I, and $\boldsymbol{j}_0$ denote the vector and scalar interpolation function, current, and unit current density, respectively. The electromagnetic field is assumed to be coupled, as expressed by the following circuit equation:

$$V = R_0 I + j\omega\,(L_0 I + \phi) \tag{3}$$

where R_0, L_0, V, and ϕ, respectively, denote the external resistance and inductance, input voltage, and magnetic flux, which is computed as $\phi = \sum_j A_j \int_\Omega \boldsymbol{N}_j \cdot \boldsymbol{j}_0 d\Omega$. We express (2) and (3) in matrix form as

$$\mathrm{K}\boldsymbol{z} + j\omega\mathrm{N}\boldsymbol{z} = V\boldsymbol{b} \tag{4a}$$

where $\mathrm{K}, \mathrm{N} \in \mathbb{R}^{m\times m}$, $\boldsymbol{z} \in \mathbb{C}^m$, $\boldsymbol{b} = [0, 0, \ldots, 1]^{\mathrm{t}} \in \mathbb{R}^m$, and m is the number of degrees of freedom in (2) and (3). In addition, the output current is expressed by

$$I = \boldsymbol{b}^{\mathrm{t}}\boldsymbol{z}. \tag{4b}$$

To obtain the transfer function that corresponds to the admittance function, denoted here by $Y(\omega)$, model order reduction techniques can be applied to (4) [4], [5]. Consequently, $Y(\omega)$ is represented by a rational function of the form

$$Y\,(\omega) = \frac{\beta_0 + \beta_1\,(j\omega) + \beta_2(j\omega)^2 + \cdots}{\alpha_0 + \alpha_1\,(j\omega) + \alpha_2(j\omega)^2 + \cdots}. \tag{5}$$

By applying the Euclid algorithm to (5), a continued fraction of the form

$$Z\ (\omega) = \frac{1}{Y\,(\omega)} = R_{\mathrm{DC}} + \cfrac{1}{\frac{1}{j\omega L_1} + \cfrac{1}{R_1 + \cfrac{1}{\frac{1}{j\omega L_2} + \cdots}}} \tag{6}$$

can be derived [5]. One can find that the continued fraction in (6) corresponds to the input impedance of the Cauer circuit shown in Fig. 1. The input–output relation of the system governed by (1) can thus be approximately represented by a Cauer circuit.

It is possible to assign a physical interpretation to the circuit parameters in the Cauer circuit. At sufficiently low frequencies, almost no current goes through R_1; most of it goes through L_1 because $j\omega L_1$ is sufficiently smaller than the impedance of the higher stages. This means that R_{DC} and L_1 correspond to the dc resistance and inductance, respectively, for the main flux without the eddy current effect. An increase in frequency gives rise to eddy current loss and a demagnetizing field due to eddy currents, which are represented by R_1 and L_2, respectively. Similarly, the effects at higher frequencies are represented by R_k $(k \geq 2)$ and L_k $(k \geq 3)$.

The principal goal of this article is to model electric devices with a Cauer circuit via measurements, not field analysis. This method is particularly useful when FE modeling is difficult because of multiple spatial scales, as in the case for devices that include litz wires or soft magnetic composites and those with materials that have uncertain characteristics.

III. Identification Method for Equivalent Circuit Parameters

To determine the circuit parameters $\boldsymbol{x} = [R_1,\ R_2, \ldots, R_{P-1}, X_1, X_2, \ldots, X_P]^{\mathrm{t}} \in \mathbb{R}^{2P-1}$ of the Cauer circuit whose stage number is P, we solve the optimization problem defined by

$$\min_{\boldsymbol{x}} F\,(\boldsymbol{x}),F\ (\boldsymbol{x}) = \sum_{q=1}^{N_{\mathrm{S}}} \left|Z\,(\boldsymbol{x}, R_{\mathrm{DC}}, \omega_q) - Z_{\mathrm{S}}\,(\omega_q)\right|^2$$

$$\text{sub. to } R_k \geq 0,\quad L_k \geq 0\quad (k = 1, 2, \ldots), \tag{7}$$

where $N_{\mathrm{S}}, \omega_q, Z(\boldsymbol{x}, R_{\mathrm{DC}}, \omega_q)$, and $Z_{\mathrm{S}}(\omega_q)$ denote the number of sampling points, qth angular frequency, impedance of the Cauer

circuit, and measured (or computed) impedance, respectively. In addition, the reactance $X_k = \omega_0\ L_k$ is defined with the maximum sampling frequency ω_0. The circuit equation for the Cauer circuit is expressed as

$$Z(\omega)\,\boldsymbol{i} \;=\; \boldsymbol{v} \tag{8a}$$

$$Z_{kl}(\omega) = \begin{cases} -j\frac{\omega}{\omega_0}X_{l-1} & (k=l-1) \\ R_{l-1} + j\frac{\omega}{\omega_0}(X_{l-1}+X_l) & (k=l) \\ -j\frac{\omega}{\omega_0}X_l & (k=l+1) \end{cases} \tag{8b}$$

$$\boldsymbol{v} = [V, 0, 0, \ldots, 0]^{\mathrm{t}} \tag{8c}$$

where V denotes the input voltage, and $R_{l-1} = R_{\mathrm{DC}}$ when $k = l = 1$. Because it is difficult to directly evaluate the sensitivity $\partial F(\boldsymbol{x})/\partial x_n$($n = 1, 2, \ldots, 2P-1$), we adopt the AVM in which the augmented objective function $\bar{F}(\boldsymbol{x})$ is minimized as follows:

$$\min_{\boldsymbol{x}} \bar{F}(\boldsymbol{x}), \bar{F}(\boldsymbol{x}) = F(\boldsymbol{x}) + \sum_{q=1}^{N_{\mathrm{S}}} \boldsymbol{\Phi}_q^{\mathrm{t}}\left(Z(\omega_q)\,\boldsymbol{i}_q - \boldsymbol{v}\right)$$
$$\text{sub. to } R_k \geq 0, \quad L_k \geq 0 \quad (k = 1, 2, \ldots), \tag{9}$$

where $\boldsymbol{\Phi}_q \in \mathbb{C}^P$ denotes the adjoint variable, which corresponds to the Lagrange multiplier in the context of nonlinear programming. Note that $\bar{F}(\boldsymbol{x}) \approx F(\boldsymbol{x})$ provided that $\boldsymbol{i}_q$ is a good approximation of the solution to (8a). The derivative of $\bar{F}(\boldsymbol{x})$ with respect to the nth circuit parameter x_n is given by

$$\frac{\partial \bar{F}(\boldsymbol{x})}{\partial x_n} = \sum_{q=1}^{N_{\mathrm{S}}}\left[\boldsymbol{\Phi}_q^{\mathrm{t}}\frac{\partial Z(\omega_q)}{\partial x_n}\boldsymbol{i}_q + \left\{\mathrm{Z}(\omega_q)\,\boldsymbol{\Phi}_q + \frac{\partial F(\boldsymbol{x})}{\partial \boldsymbol{i}_q}\right\}^{\mathrm{t}}\frac{\partial \boldsymbol{i}_q}{\partial x_n}\right] \tag{10}$$

where it is assumed that the current $\boldsymbol{i}_q$ is an implicit function of x_n. It is difficult to directly evaluate the second term in (10). To eliminate it, we solve the adjoint equations

$$Z(\omega_q)\,\boldsymbol{\Phi}_q = -\frac{\partial F(\boldsymbol{x})}{\partial \boldsymbol{i}_q}, q = 1, 2, \ldots, N_s \tag{11}$$

to obtain the adjoint variable $\boldsymbol{\Phi}_q$. By substituting $\boldsymbol{\Phi}_q$ into the first term in (10), we can obtain the derivative of $\bar{F}(\boldsymbol{x})$. Here, the right-hand side in (11) needs to be carefully treated because there it is no guarantee that $F(\boldsymbol{x})$ is a holomorphic function that satisfies the Cauchy–Riemann equations

$$\frac{\partial F^r(\boldsymbol{x})}{\partial \boldsymbol{i}_q^r} = \frac{\partial F^i(\boldsymbol{x})}{\partial \boldsymbol{i}_q^i} \tag{12a}$$

$$\frac{\partial F^r(\boldsymbol{x})}{\partial \boldsymbol{i}_q^i} = -\frac{\partial F^i(\boldsymbol{x})}{\partial \boldsymbol{i}_q^r} \tag{12b}$$

where the superscripts r and i denote the real and imaginary parts, respectively. For this reason, we apply the complex AVM [25], [26] so that (11) is modified to

$$Z(\omega_q)\ \boldsymbol{\Phi}_q = \frac{\partial F(\boldsymbol{x})}{\partial \boldsymbol{i}_q^r}\ - \mathrm{j}\frac{\partial F(\boldsymbol{x})}{\partial \boldsymbol{i}_q^i} \tag{13}$$

where the right-hand side in (13) is computed only with respect to the circuit current of the first stage i_{1q} because the input impedance of the Cauer circuit can be evaluated as $Z(\boldsymbol{x}, R_{\mathrm{DC}}, \omega_q) = V/i_{1q}$. The derivative of $\bar{F}(\boldsymbol{x})$ is now given by [26]

$$\frac{\partial \bar{F}(\boldsymbol{x})}{\partial x_n} = -\mathrm{Re}\left(\sum_{q=1}^{N_{\mathrm{S}}} \boldsymbol{i}_q^{\mathrm{t}}\frac{\partial Z(\omega_q)}{\partial x_n}\boldsymbol{\Phi}_q\right). \tag{14}$$

In addition, we impose a constraint on $\bar{F}(\boldsymbol{x})$ so that the resultant circuit parameters take nonnegative values. To do so, the constraint functions $g_k(\boldsymbol{x})$, $k = 1, 2, \ldots$, are introduced on the basis of the augmented Lagrangian method [27] as follows:

$$\min_{\boldsymbol{x}} M(\boldsymbol{x}, \boldsymbol{\lambda}; r)$$
$$M(\boldsymbol{x}, \boldsymbol{\lambda}; r) = F(\boldsymbol{x}) + \sum_{q=1}^{N_{\mathrm{S}}} \boldsymbol{\Phi}_q^{\mathrm{t}}\left(Z(\omega_q)\,\boldsymbol{i}_q - \boldsymbol{v}\right)$$
$$+ \frac{1}{4r}\sum_k \left[\left\{\min\left(0, 2rg_k(\boldsymbol{x}) + \lambda_k\right)\right\}^2 - \left(\lambda_k\right)^2\right] \tag{15}$$

where r and $\boldsymbol{\lambda}$ denote the penalty coefficient and Lagrangian multiplier, respectively. The derivative of $M(\boldsymbol{x}, \boldsymbol{\lambda}; r)$ is given by

$$\frac{\partial M(\boldsymbol{x}, \boldsymbol{\lambda}; r)}{\partial x_n} = -\mathrm{Re}\left(\sum_{q=1}^{N_{\mathrm{S}}} \boldsymbol{i}_q^{\mathrm{t}}\frac{\partial Z(\omega_q)}{\partial x_n}\boldsymbol{\Phi}_q\right)$$
$$+ \frac{1}{2r}\sum_k \left[\min\left(0, 2rg_k(\boldsymbol{x}) + \lambda_k\right)\min\left(0, 2r\frac{\partial g_k(\boldsymbol{x})}{\partial x_n}\right)\right]. \tag{16}$$

To update the circuit parameters using (16), the quasi-Newton method based on the Broyden–Fletcher–Goldfarb–Shanno algorithm is employed in this work. The above process is schematically shown in Fig. 2.

IV. Numerical Results

A. Frequency Characteristics and Circuit Parameters

Although the proposed method can be applied to various electric devices, we confine ourselves to inductor and reactor models for the verification. Let us first consider the simple inductor model shown in Fig. 3 whose input impedance is analyzed using the FE method. We compare the performance of the proposed method with that of the conventional circuit parameter identification using the GA [12]–[17]. The parameters for the proposed method and the GA are summarized in Tables I and II, respectively. The results are plotted in Fig. 4. The input resistance and reactance values computed from the equivalent circuits whose parameters were determined by the two approaches agree well with those computed from the FE analysis over the frequency range of interest. Because the skin depth, about 0.15 mm at the highest frequency (200 kHz), is larger than the strand radius, the proximity effect is stronger than the skin effect.

The corresponding fitting errors for both methods are plotted in Fig. 5. It can be concluded that the proposed method has smaller fitting errors in comparison with GA for this model.

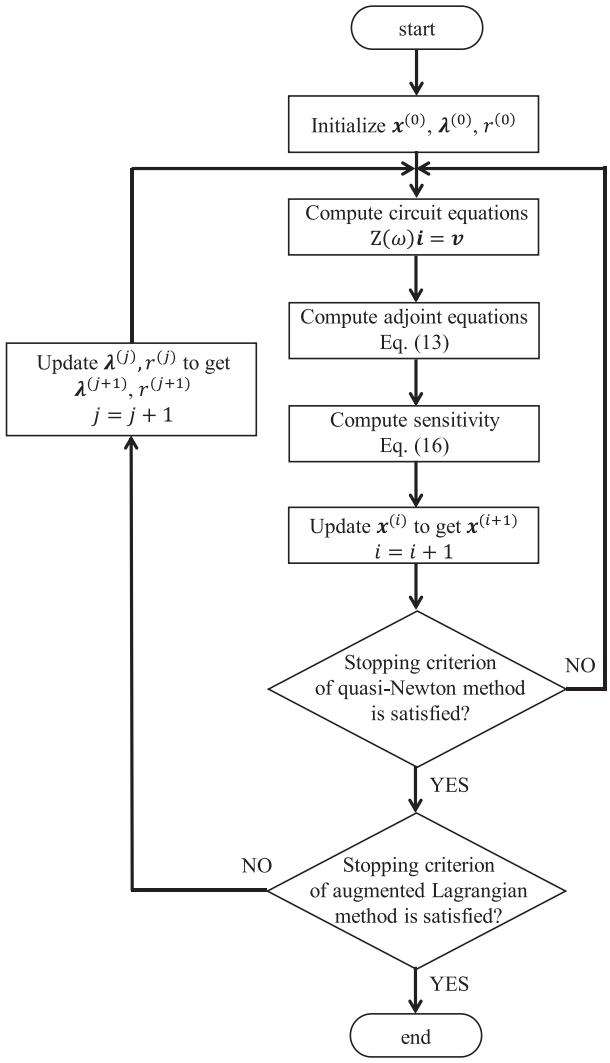

Fig. 2. Flow diagram of the proposed method.

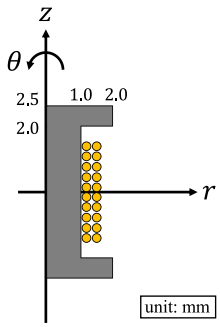

Fig. 3. 20-turn inductor model (strand radius: 0.15 mm, relative permeability of the magnetic core: 1000, conductivity of the strand: 5.76×10^7 S/m).

TABLE I
OPTIMIZATION PARAMETERS FOR THE PROPOSED METHOD

Initial circuit parameter $x_n^{(0)}$	1.0 Ω
Initial multiplier value $\lambda_n^{(0)}$	0.0
Initial penalty parameter $r^{(0)}$	5.0
Stopping criterion of the quasi-Newton method	$\left\lvert\frac{\partial M(\boldsymbol{x},\boldsymbol{\lambda},r)}{\partial \boldsymbol{x}}\right\rvert < 10^{-8}$
Stopping criterion of the augmented Lagrangian method	$\lvert\min\{\boldsymbol{g}(\boldsymbol{x}), \quad -\boldsymbol{\lambda}/2r\}\rvert < 10^{-6}$

TABLE II
OPTIMIZATION PARAMETERS FOR GA

Number of generations	10,000
Number of populations[1]	$50 \times (2P - 1)$

Note that P denotes the number of stages of the Cauer circuit shown in Fig. 1.

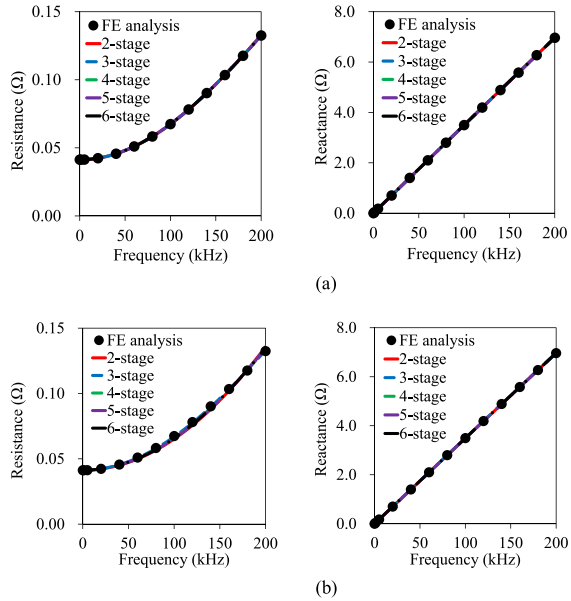

Fig. 4. Frequency characteristics of equivalent circuits obtained with (a) proposed method and (b) GA.

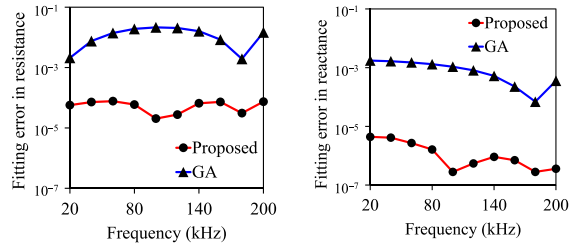

Fig. 5. Fitting errors with a four–stage circuit.

The convergence histories are shown in Fig. 6. The circuit parameters after convergence for the proposed method and the GA are summarized in Tables III and IV, respectively. The value of R_{DC} is precomputed from the geometry of the model shown in Fig. 3 without curve fitting. We found that the squared error for the proposed method shown in Fig. 6(a) decreases to about 5.0×10^{-10} when the number of circuit stages P is greater than 4. In contrast, the squared error for the GA shown in Fig. 6(b) tends to stagnate at around 10^{-4} regardless of P, even though the evolution process was continued for over 10 000 generations. In addition, the synthesized circuit parameters determined from

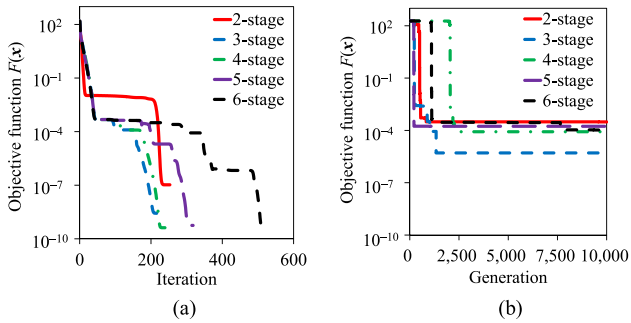

Fig. 6. Convergence histories for (a) proposed method and (b) GA.

TABLE III
CIRCUIT PARAMETERS DETERMINED FROM THE PROPOSED METHOD

	Number of circuit stages				
	2	3	4	5	6
R_{DC} (Ω)	4.13×10^{-2}	4.13×10^{-2}	4.13×10^{-2}	4.13×10^{-2}	4.13×10^{-2}
R_1 (Ω)	4.49×10^{2}	4.45×10^{2}	4.45×10^{2}	4.46×10^{2}	4.46×10^{2}
R_2 (Ω)		6.20×10^{3}	6.77×10^{3}	3.14×10^{3}	9.01×10^{3}
R_3 (Ω)			1.23×10^{3}	6.02×10^{3}	1.03×10^{4}
R_4 (Ω)				2.23×10^{4}	1.45×10^{1}
R_5 (Ω)					6.78×10^{-4}
L_1 (H)	5.57×10^{-6}	5.57×10^{-6}	5.57×10^{-6}	5.57×10^{-6}	5.57×10^{-6}
L_2 (H)	1.53×10^{-4}	1.55×10^{-4}	1.54×10^{-4}	1.54×10^{-4}	1.53×10^{-4}
L_3 (H)		2.93×10^{-3}	6.61×10^{-2}	9.48×10^{-3}	4.02×10^{-4}
L_4 (H)			2.18×10^{-3}	2.72×10^{-5}	3.82×10^{-3}
L_5 (H)				6.45×10^{-7}	4.32×10^{-6}
L_6 (H)					7.44×10^{-5}

TABLE IV
CIRCUIT PARAMETERS DETERMINED FROM GA

	Number of circuit stages				
	2	3	4	5	6
R_{DC} (Ω)	4.13×10^{-2}	4.13×10^{-2}	4.13×10^{-2}	4.13×10^{-2}	4.13×10^{-2}
R_1 (Ω)	5.08×10^{2}	4.60×10^{2}	4.85×10^{2}	4.96×10^{2}	4.91×10^{2}
R_2 (Ω)		2.61×10^{0}	4.48×10^{3}	2.04×10^{3}	8.34×10^{4}
R_3 (Ω)			1.64×10^{18}	8.3×10^{133}	9.28×10^{3}
R_4 (Ω)				1.3×10^{137}	9.06×10^{4}
R_5 (Ω)					2.8×10^{150}
L_1 (H)	5.56×10^{-6}	5.57×10^{-6}	5.56×10^{-6}	5.56×10^{-6}	5.56×10^{-6}
L_2 (H)	4.45×10^{-5}	1.41×10^{-4}	1.01×10^{-4}	7.48×10^{-5}	9.35×10^{-5}
L_3 (H)		7.61×10^{-1}	2.8×10^{-15}	7.5×10^{-17}	7.1×10^{-12}
L_4 (H)			6.12×10^{0}	1.9×10^{117}	9.24×10^{-7}
L_5 (H)				8.1×10^{119}	4.0×10^{-12}
L_6 (H)					4.6×10^{140}

the GA include extraordinarily large values (e.g., $R_4 = 1.3 \times 10^{137}$ Ω) due to the stochastic nature of the algorithm.

B. Dependence of Settings on Convergence

In order to study the dependence of the convergence of the proposed method and GA on the initial guess and hyperparameters, we perform the circuit identification under different

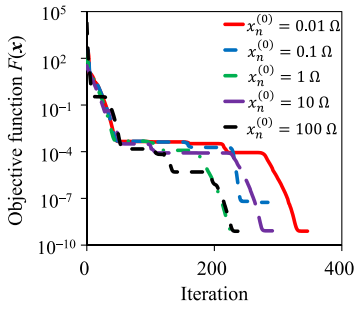

Fig. 7. Dependence of initial parameters on convergence for the proposed method.

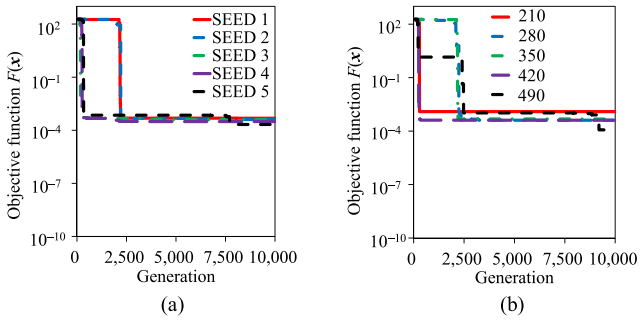

Fig. 8. Dependence of hyperparameters on convergence of GA. Convergence for different number of populations is shown in (b). (a) Random seed. (b) Number of populations.

settings. The convergence histories for a four-stage circuit are plotted for the five cases in Figs. 7 and 8. We can see that the squared errors for the proposed method shown in Fig. 7 decrease to about 5.0×10^{-10} regardless of the initial circuit parameter. In contrast, the squared error for GA shown in Fig. 8 tends to stagnate at around 10^{-4} even when the random seed and number of populations, which is chosen 30 times larger than the number of unknowns at least, are changed.

C. High-Frequency Characteristics of Equivalent Circuit

The Cauer circuit model was evaluated at a frequency that is above the highest frequency (200 kHz) considered for the curve fitting. The frequency characteristics of the input impedance of the Cauer circuit up to 1 MHz are plotted in Fig. 9, where the circuit parameters were identified using the proposed method and the GA. It can be seen that the Cauer circuit works well over the frequency range with a rather small stage number when the proposed method is applied. In contrast, the GA requires a greater number of stages for the identified Cauer circuit. The results demonstrate the superiority of the proposed method for the considered problem.

V. EXPERIMENTAL VALIDATION AND SIMULATED TIME RESPONSE

A. Circuit Identification

The proposed method was used to identify the Cauer circuit parameters from the measured input impedance of the reactor

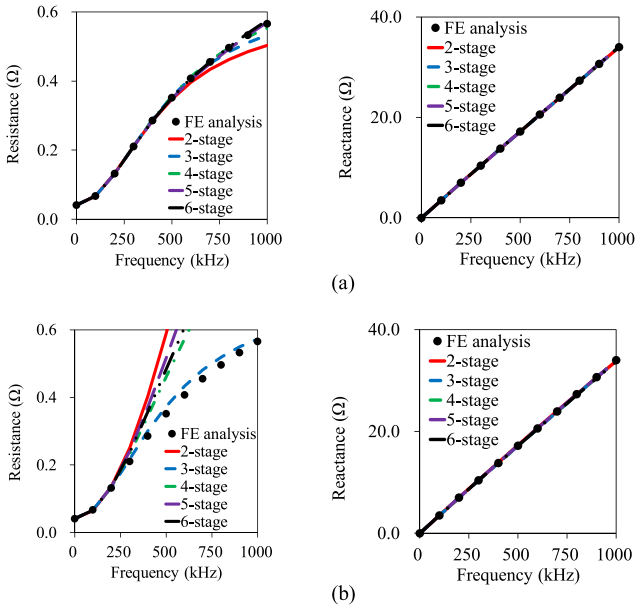

Fig. 9. High-frequency characteristics of equivalent circuits obtained with (a) proposed method and (b) GA.

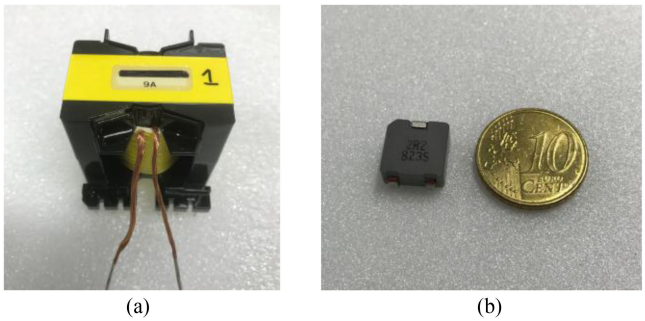

Fig. 10. Reactor and power inductor for experimental validation. (a) Reactor with ten-turn litz wire. (b) Power inductor [28].

TABLE V
SPECIFICATIONS OF REACTOR WITH TEN-TURN LITZ WIRE

Number of strands	12
Strand radius	0.16 mm
Twist pitch	20 mm
Magnetic core type	PQ 50/50
Magnetic core material	PC47
Air gap in magnetic core	0.3 mm

with ten-turn litz wire and power inductor used in, e.g., a dc–dc converter [28] shown in Fig. 10. Table V summarizes specifications of the reactor. The frequency characteristics of the input impedance are plotted in Fig. 11.

The ac resistance and reactance were measured with an *LCR* meter (HIOKI IM3523), where the signal level for the measurements was set to 10 mA to exclude the magnetic core losses. The resistance and reactance computed from the identified Cauer circuit parameters agree well with those obtained from the measurements. The resultant circuit parameters are summarized

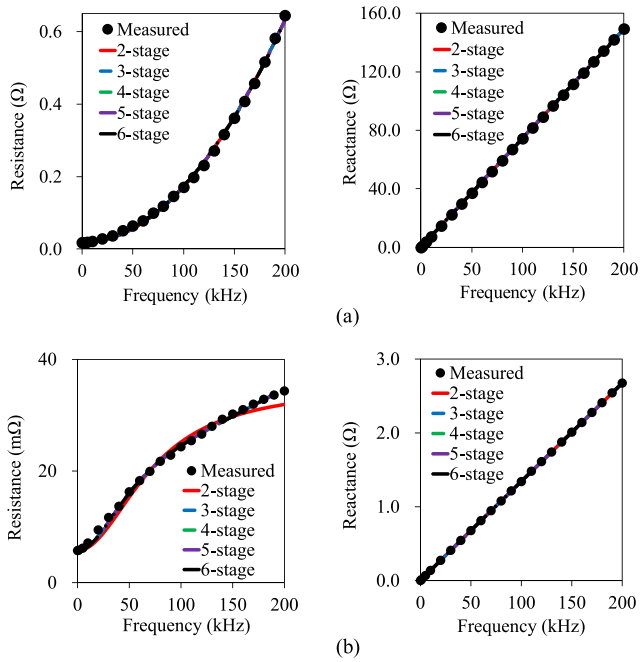

Fig. 11. Frequency dependence of reactor and power inductor. (a) Reactor with ten-turn litz wire. (b) Power inductor.

TABLE VI
IDENTIFIED CIRCUIT PARAMETERS FOR REACTOR WITH TEN-TURN LITZ WIRE

	Number of circuit stages				
	2	3	4	5	6
R_{DC} (Ω)	1.85×10^{-2}	1.85×10^{-2}	1.85×10^{-2}	1.85×10^{-2}	1.85×10^{-2}
R_1 (Ω)	3.61×10^{4}	3.61×10^{4}	3.61×10^{4}	3.61×10^{4}	2.50×10^{-3}
R_2 (Ω)		2.27×10^{1}	1.16×10^{-5}	6.41×10^{4}	3.63×10^{4}
R_3 (Ω)			1.87×10^{2}	5.48×10^{3}	1.86×10^{4}
R_4 (Ω)				7.43×10^{2}	3.02×10^{3}
R_5 (Ω)					2.14×10^{3}
L_1 (H)	1.19×10^{-4}	1.19×10^{-4}	1.19×10^{-4}	1.19×10^{-4}	7.30×10^{-3}
L_2 (H)	-1.6×10^{-13}	8.62×10^{-3}	2.97×10^{-2}	-1.6×10^{-13}	1.21×10^{-4}
L_3 (H)		-1.6×10^{-13}	-1.6×10^{-13}	7.08×10^{-3}	-1.6×10^{-13}
L_4 (H)			8.10×10^{-3}	1.40×10^{-3}	1.58×10^{-4}
L_5 (H)				7.68×10^{-4}	3.97×10^{-3}
L_6 (H)					1.03×10^{-3}

in Tables VI and VII and the convergence histories are shown in Fig. 12. The converged values in Fig. 12(a) plateau at about 1.0, whereas those in Figs. 6(a) and 12(b) continue to decrease. This might be due to the measurement errors that cannot be well approximated by the Cauer circuit.

B. Computation of Time Response

As an application of the proposed method, we computed the time evolution of the eddy current loss in the ten-turn reactor using the identified Cauer circuit parameters. The test circuit 1 with a sinusoidal input voltage is shown in Fig. 13 where Z_p denotes the parasitic impedance of C and R_{LOAD}. The time response was computed with the software LTspice

TABLE VII
IDENTIFIED CIRCUIT PARAMETERS FOR POWER INDUCTOR

	Number of circuit stages				
	2	3	4	5	6
R_{DC} (Ω)	5.73×10^{-3}	5.73×10^{-3}	5.73×10^{-3}	5.73×10^{-3}	5.73×10^{-3}
R_1 (Ω)	3.32×10^{1}	2.58×10^{1}	2.56×10^{1}	2.57×10^{1}	2.57×10^{1}
R_2 (Ω)		7.70×10^{2}	7.68×10^{2}	7.69×10^{2}	7.15×10^{2}
R_3 (Ω)			5.62×10^{-3}	2.05×10^{-2}	5.48×10^{1}
R_4 (Ω)				4.03×10^{-1}	1.96×10^{0}
R_5 (Ω)					2.25×10^{0}
L_1 (H)	2.18×10^{-6}	2.19×10^{-6}	2.19×10^{-6}	2.19×10^{-6}	2.19×10^{-6}
L_2 (H)	7.10×10^{-5}	6.99×10^{-5}	6.99×10^{-5}	6.99×10^{-5}	7.00×10^{-5}
L_3 (H)		4.95×10^{-9}	4.50×10^{-5}	2.70×10^{-5}	1.56×10^{-4}
L_4 (H)			3.91×10^{-5}	1.06×10^{-5}	2.26×10^{-5}
L_5 (H)				1.82×10^{-5}	1.21×10^{-16}
L_6 (H)					1.61×10^{-7}

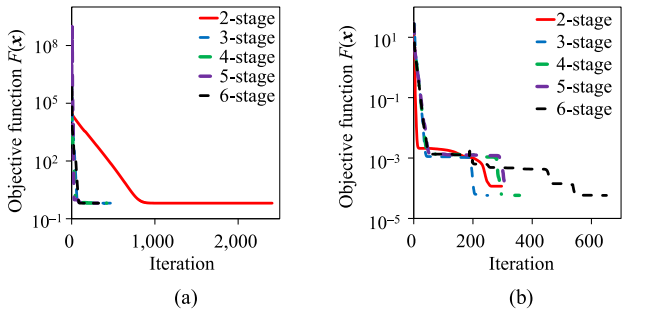

Fig. 12. Convergence history for reactor and power inductor. (a) Reactor with ten-turn litz wire. (b) Power inductor.

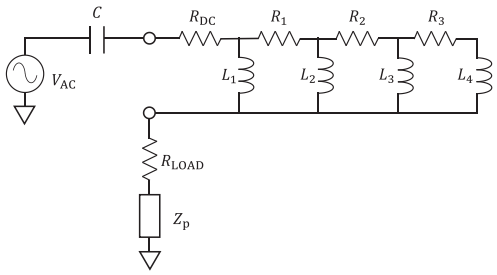

Fig. 13. Test circuit 1 for transient analysis (V_{AC} = –11 to 11 V, frequency = 183 kHz, C = 6 nF, R_{LOAD} = 5Ω, $Z_p = 1.4 + j1.6\Omega$).

TABLE VIII
SIMULATED AND MEASURED ACTIVE POWERS OF R_{LOAD}

Measured	3.76 W
Proposed	3.91 W
Conventional	4.21 W

and measured with a power analyzer (HIOKI PW6001). We take the absolute value of L_3, negative value close to zero, in the simulation to stabilize the circuit behavior. The transient responses of the ten-turn reactor and load resistance are plotted in Fig. 14. Table VIII summarizes the simulated and measured active powers of R_{LOAD}. The loss in the proposed circuit shown

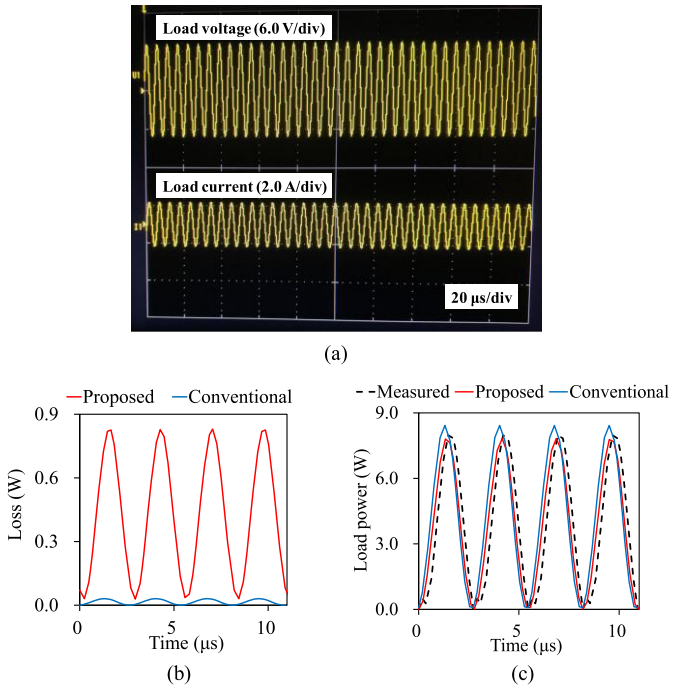

Fig. 14. Transient responses for test circuit 1. (a) Measured results of load voltage and load current. (b) Loss of ten-turn reactor. (c) Load power.

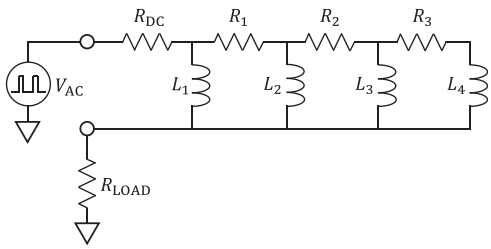

Fig. 15. Test circuit 2 for transient analysis (V_{AC} = –10 to 10 V, period = 10 μs, duty = 50%, R_{LOAD} = 5.0 Ω).

in Fig. 14(b) is mainly contributed from R_{DC} and R_1. It is found that the relative error between the active powers obtained from the proposed circuit and measurement is less than 5%, whereas the relative error for the conventional circuit is greater than 10%, in which the eddy current loss is not considered.

In order to apply the proposed circuit to practical electric devices, such as a dc–dc converter, we consider, here, the test circuit 2 with a pulsed input voltage as shown in Fig. 15. The transient losses of the reactor are plotted in Fig. 16. It can be seen that the loss evaluated using the proposed circuit is greater than that of the simple circuit due to the eddy current loss.

C. Discussion

The losses due to eddy currents and circulating current in the multiturn litz wire coils have to be considered at high frequencies. Numerical methods have been proposed to evaluate these effects considering the bundling and twisting structures in the winding coils [29]–[32]. An experimental method for extracting the ac resistance in a transformer with litz wire has

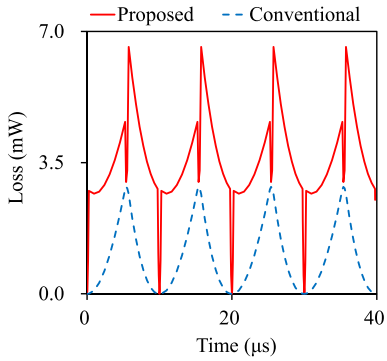

Fig. 16. Transient losses of ten-turn reactor in test circuit 2.

been proposed, where the geometric tolerance in the litz wire is directly considered [33]. This experimental method is more practical because accurate information on internal components in electric devices is often unavailable.

For such cases, even if the internal device structure is unknown, the circuit model with eddy current effects, which can be readily embedded into circuit simulators, can be constructed using the proposed method.

VI. Conclusion

In this article, we proposed a method for modeling electric devices using the Cauer equivalent circuit considering the eddy current losses. The circuit parameters are directly determined from measured data using AVM. The proposed method was demonstrated to outperform a conventional method using a GA for the FE model of a simple inductor. Moreover, the proposed method was shown to be valid for the identification of Cauer circuit parameters from the measured input impedance of a reactor with litz wire and a power inductor.

The validity of the proposed method for the modeling of windings in electric motors and generators should be verified in future studies. Moreover, the validity for devices with saturable magnetic cores should be examined.

Acknowledgment

The authors would like to thank A. Przywecki, from Edanz Group, for editing a draft of this article.

References

[1] T. Miyazaki, T. Mifune, T. Matsuo, Y. Shindo, Y. Takahashi, and K. Fujiwara, "Equivalent circuit modeling of dynamic hysteretic property of silicon steel under pulse width modulation excitation," *J. Appl. Phys.*, vol. 117, 2015, Art. no. 17D110.

[2] Y. Shindo and O. Noro, "Simple circuit simulation models for eddy current in magnetic sheets and wires," *IEE J. Trans. Fundam. Mater.*, vol. 134, no. 4, pp. 173–181, 2014.

[3] E. J. Tarasiewicz, A. S. Morched, A. Narang, and E. P. Dick, "Frequency dependent eddy current models for nonlinear iron cores," *IEEE Trans. Power Syst.*, vol. 8, no. 2, pp. 588–597, May 1993.

[4] Y. Sato and H. Igarashi, "Generation of equivalent circuit from finite-element model using model order reduction," *IEEE Trans. Magn.*, vol. 52, no. 3, Mar. 2016, Art. no. 1100304.

[5] Y. Sato, T. Shimotani, and H. Igarashi, "Synthesis of Cauer-equivalent circuit based on model order reduction considering nonlinear magnetic property," *IEEE Trans. Magn.*, vol. 53, no. 6, Jun. 2017, Art. no. 1100204.

[6] T. Shimotani, Y. Sato, and H. Igarashi, "Direct synthesis of equivalent circuits from reduced FE models using proper orthogonal decomposition," *COMPEL*, vol. 35, no. 6, pp. 2035–2044, 2016.

[7] S. Hiruma and H. Igarashi, "Model order reduction for linear time-invariant system with symmetric positive-definite matrices: Synthesis of Cauer-equivalent circuit," *IEEE Trans. Magn.*, vol. 56, no. 3, Mar. 2020, Art. no. 7400608.

[8] A. Kameari, H. Ebrahimi, K. Sugahara, Y. Shindo, and T. Matsuo, "Cauer ladder network representation of eddy-current fields for model order reduction using finite-element method," *IEEE Trans. Magn.*, vol. 54, no. 3, Mar. 2018, Art. no. 7201804.

[9] T. Matsuo, K. Sugahara, A. Kameari, and Y. Shindo, "Model order reduction of an induction motor using a Cauer ladder network," *IEEE Trans. Magn.*, vol. 56, no. 3, Mar. 2020, Art. no. 7514704.

[10] N. Minowa, Y. Takahashi, and K. Fujiwara, "Iron loss analysis of interior permanent magnet synchronous motors using dynamic hysteresis model represented by Cauer circuit," *IEEE Trans. Magn.*, vol. 55, no. 6, 2019, Art. no. 7401404.

[11] A. A. Moya, "A ladder network modeling the electrochemical impedance of the diffusion and reaction processes in semi-infinite space," *Phys. Chem. Chem. Phys.*, vol. 18, no. 5, pp. 3812–3816, 2016.

[12] P. Mukherjee and L. Satish, "Construction of equivalent circuit of a single and isolated transformer winding from FRA data using the ABC algorithm," *IEEE Trans. Power Del.*, vol. 27, no. 2, pp. 963–970, Apr. 2012.

[13] N. V. Korovkin, V. L. Chechurin, and M. Hayakawa, *Inverse Problems in Electric Circuits and Electromagnetics*. New York, NY, USA: Springer, 2007, ch. 5, pp. 275–285.

[14] M. M. Shabestary, A. J. Ghanizadeh, G. B. Gharehpetian, and M. Agha-Mirsalim, "Ladder network parameters determination considering non-dominant resonances of the transformer winding," *IEEE Trans. Power Del.*, vol. 29, no. 1, pp. 108–117, Feb. 2014.

[15] A. Shintemirov, W. H. Tang, and Q. H. Wu, "Transformer core parameter identification using frequency response analysis," *IEEE Trans. Magn.*, vol. 46, no. 1, pp. 141–149, Jan. 2010.

[16] V. Rashtchi, E. Rahimpour, and E. M. Rezapour, "Using a genetic algorithm for parameter identification of transformer R-L-C-M model," *Elect. Eng.*, vol. 88, no. 5, pp. 417–422, 2006.

[17] Y. Otomo, Y. Sato, S. Fujita, and H. Igarashi, "Synthesis of equivalent circuit of wireless power transfer device using homogenization-based FEM," *IEEE Trans. Magn.*, vol. 54, no. 3, Mar. 2018, Art. no. 7401005.

[18] T. Shimotani, H. Igarashi, E. Hashimoto, and H. Imanari, "Equivalent circuit allowing loss separation synthesized from field computations: Application to induction heating," *IEEE Trans. Magn.*, vol. 56, no. 2, Feb. 2020, Art. no. 7505405.

[19] S. W. Director and R. A. Rohrer, "The generalized adjoint network and network sensitivities," *IEEE Trans. Circuit Theory*, vol. CT-16, no. 3, pp. 318–323, Aug. 1969.

[20] S. W. Director and R. A. Rohrer, "Automated network design–the frequency–domain case," *IEEE Trans. Circuit Theory*, vol. CT-16, no. 3, pp. 330–337, Aug. 1969.

[21] P. Penfield, R. Spence, and S. Duinker, "A generalized form of Tellegen's theorem," *IEEE Trans. Circuit Theory*, vol. CT-17, no. 3, pp. 302–305, Aug. 1970.

[22] V. A. Monaco and P. Tiberio, "Computer-aided analysis of microwave circuits," *IEEE Trans. Microw. Theory Techn.*, vol. MTT-22, no. 3, pp. 249–263, Mar. 1974.

[23] Z. Ren, H. Qu, and X. Xu, "Computation of second order capacitance sensitivity using adjoint method in finite element modeling," *IEEE Trans. Magn.*, vol. 48, no. 2, pp. 231–234, Feb. 2012.

[24] S. Barmada, A. Musolino, R. Rizzo, and M. Tucci, "Multi-resolution based sensitivity analysis of complex non-linear circuits," *IET Circuits Devices Syst.*, vol. 6, no. 3, pp. 176–186, 2012.

[25] N. K. Nikolova, J. W. Bandler, and M. H. Bakr, "Adjoint techniques for sensitivity analysis in high-frequency structure CAD," *IEEE Trans. Microw. Theory Techn.*, vol. 52, no. 1, pp. 403–419, Jan. 2004.

[26] H. Igarashi and K. Watanabe, "Complex adjoint variable method for finite-element analysis of eddy current problems," *IEEE Trans. Magn.*, vol. 46, no. 8, pp. 2739–2742, Aug. 2010.

[27] J. Nocedal and S. J. Wright, *Numerical Optimization*. New York, NY, USA: Springer, 2006, ch. 17, pp. 497–528.

[28] Murata Manufacturing Co., Ltd., "FDA1055-H-2R2M," Sep. 2018. [Online]. Available: https://www.murata.com/en-global/products/productdetail?partno=FDA1055-H-2R2M%23, Accessed: Jun. 14, 2020.
[29] A. Roßkopf, E. Bär, C. Joffe, and C. Bonse, "Calculation of power losses in litz wire systems by coupling FEM and PEEC method," *IEEE Trans. Power Electron.*, vol. 31, no. 9, pp. 6442–6449, Sep. 2016.
[30] S. Hiruma, Y. Otomo, and H. Igarashi, "Eddy current analysis of litz wire using homogenization-based FEM in conjunction with integral equation," *IEEE Trans. Magn.*, vol. 54, no. 3, Mar. 2018, Art. no. 7001404.
[31] S. Gyimóthy *et al.*, "Loss computation method for litz cables with emphasis on bundle-level skin effect," *IEEE Trans. Magn.*, vol. 55, no. 6, Jun. 2019, Art. no. 6300304.
[32] T. Guillod, J. Huber, F. Krismer, and J. W. Kolar, "Litz wire losses: Effects of twisting imperfections," in *Proc. IEEE Control Model. Power Electron. Conf.*, 2017, pp. 1–8.
[33] K. Niyomsatian, J. Gyselinck, and R. V. Sabariego, "Experimental extraction of winding resistance in litz-wire transformers—Influence of winding mutual resistance," *IEEE Trans. Power Electron.*, vol. 34, no. 7, pp. 6736–6746, Jul. 2019.

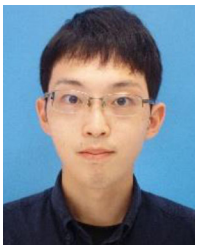

Yoshitsugu Otomo received the B.E. and M.I.S. degrees in electrical engineering from Hokkaido University, Sapporo, Japan, in 2017 and 2019, respectively.

He is currently a Doctoral Student with the Graduate School of Information Science and Technology, Hokkaido University. His current research interests include computational electromagnetism and design optimization.

Mr. Otomo is currently a Research Fellow of the Japan Society for Promotion of Science.

Hajime Igarashi (Member, IEEE) received the B.E. and M.E. degrees in electrical engineering and the Ph.D. degree in engineering from Hokkaido University, Sapporo, Japan, in 1982, 1984, and 1992, respectively.

He has been a Professor with the Graduate School of Information Science and Technology, Hokkaido University, since 2004. His research areas include computational electromagnetism, design optimization, and energy harvesting.

Dr. Igarashi is a member of the International COMPUMAG Society, the Japan Society for Simulation Technology, the Japan Society for Computational Methods in Engineering, and the Japan Society of Applied Electromagnetics and Mechanics. He was the recipient of the Outstanding Technical Paper Award by The Institute of Electrical Engineers of Japan in 2016.